 doi:10.20944/preprints202005.0496.v1

Article

Exploring the Potential of β-Catenin *O*-GlcNAcylation by Using Fluorescence-Based Engineering and Imaging

Angelina Kasprowicz [1], Corentin Spriet [1,2], Christine Terryn [3], Matthew G. Alteen [4], Tony Lefebvre [1] and Christophe Biot [1,*]

1 Univ. Lille, CNRS, UMR 8576 – UGSF – Unité de Glycobiologie Structurale et Fonctionnelle 59000 Lille (France); angelina.kasprowicz@univ-lille.fr (A.K.); corentin.spriet@univ-lille.fr (C.S.); tony.lefebvre@univ-lille.fr (T.L.); christophe.biot@univ-lille.fr (C.B.)
2 Univ. Lille, CNRS, UMS 2014 - US 41 - Plateformes Lilloises en Biologie & Santé. 59000 Lille (France); corentin.spriet@univ-lille.fr (C.S.)
3 PICT Platform, University of Reims Champagne-Ardenne, 51 rue Cognacq-Jay, 51100, Reims (France); christine.terryn@univ-reims.fr (C.T.)
4 Department of Chemistry, Department of Molecular Biology and Biochemistry, Simon Fraser University, Burnaby (Canada) ; malteen@sfu.ca (M.A.)

* Correspondence: christophe.biot@univ-lille.fr; Tel.: +33 (0)3 20 43 61 41

Abstract:
Monitoring glycosylation changes within cells upon response to stimuli remains challenging because of the complexity of this large family of post-translational modifications (PTMs). We have developed an original tool enabling labeling and visualization of the cell cycle key-regulator β-catenin in its *O*-GlcNAcylated form based on intramolecular Förster resonance energy transfer (FRET) technology in cells. We opted for a bioorthogonal chemical reporter strategy based on the dual-labeling of β-catenin with a green fluorescent protein (GFP) for protein sequence combined with a chemically-clicked imaging probe for PTM resulting in a fast and easy to monitor qualitative FRET assay. We validated this technology by imaging the *O*-GlcNAcylation status of β-catenin in HeLa cells. Moreover, the changes in *O*-GlcNAcylation of β-catenin were varied by perturbing global cellular *O*-GlcNAc levels with inhibitors of *O*-GlcNAc transferase (OGT) and *O*-GlcNAcase (OGA). Finally, we provided a flowchart demonstrating how this technology is transposable to any kind of glycosylation.

Keywords: bioorthogonal chemistry, fluorescence, glycosylation, metabolic incorporation, GFP, β-catenin.

1. Introduction

The complete set of glycans, i.e. the glycome, represents a large diversity of structures and functions, and plays a central role in biology and health [1]. Glycans are involved in many biological processes such as protein folding and traffic, cell-to-cell recognition, immune defense, or cell protection [1]. Glycans are also specific markers for numerous pathologies including, most notably, cancers [2]. This functional diversity is linked to great structural diversity. Indeed, a wide variety of different forms of glycosylation are possible and, moreover, variation in glycosylation of the same protein within tissues occurs leading to various "glycoforms" of a given protein glycoforms [3].

The various forms of glycosylation is essential for cell homeostasis, in this regard it is considered that 2% of the human genome is devoted to glycosylation. The most complex forms of glycosylation, namely *N*-linked protein, *O*-linked protein, and *O*-linked mucin-type glycosylation, take place

mainly in the endoplasmic *reticulum* and the Golgi apparatus where the requisite biosynthetic enzymes residue. Another widespread form of glycosylation is *O*-linked β-*N*-acetylglucosaminylation (*O*-GlcNAcylation) [4]. *O*-GlcNAcylation is much more simple than glycosylation occurring within the secretory pathway and consists of the modification of cytoplasmic, nuclear and mitochondrial proteins with a single residue of *N*-acetylglucosamine (GlcNAc). Further, in contrast to the more complex glycosylation of the secretory pathway, *O*-GlcNAcylation is highly dynamic, its versatility being managed by a unique couple of enzymes, *O*-GlcNAc transferase (OGT) and *O*-GlcNAcase (OGA), which respectively install and removes the GlcNAc moiety on and off targeted substrate proteins [5].

During the last three decades, Metabolic Oligosaccharide Engineering (MOE, also termed Metabolic GlycoEngineering (MGE)) paved the way for the manipulation of biosynthetic pathways responsible for oligosaccharides and glycoconjugates production [6–9]. MOE exploits the substrate promiscuity of different glycosylation pathways to incorporate non-natural monosaccharides into cellular glycans. Upon metabolization, the non-natural saccharides are detected with a complementary probe through bioorthogonal ligation. This technology has been mostly used for labeling cell surface-exposed glycoconjugates especially with fluorescent probes [6,7], but there are some intra-cellular MOE applications, notably targeting *O*-GlcNAc.

However, these strategies usually aim to report for the general glycosylation status of a cell and, to date, only a few MOE methods have been reported that account for the glycosylation pattern of a single specific glycoprotein. The five examples are based on dual-labeling strategies exploiting Förster resonance energy transfer (FRET). Haga and coworkers used azido sialic acid (SiaNAz) labeling of GLUT4-GFP to image cell surface glycoproteins [3]. Belardi and coworkers developed a technique using Ac_4ManNAz (the precursor of SiaNAz) to study the vitronectin receptor $\alpha_v\beta_3$ after targeting with a donor fluorophore-labeled Fab fragment [10]. The dual-labeling of membrane proteins developed by Lin and coworkers relies on two bioorthogonal chemical reporters delivered one to the protein and the other to the glycan [11]. Surprisingly, only modest progresses have been made in studying intracellular glycosylation with *O*-GlcNAc. The two examples to visualize *O*-GlcNAcylation in a protein-specific manner has been also reported by Lin and coworkers [12], and Doll and coworkers [13].

Herein, we present optimized methods for probing the glycosylation state of β-catenin within HeLa cells using fluorescence-based imaging. β-catenin plays many critical functions in animals. First, Wnt/β-catenin signaling – for which the protein is the central component - is actively involved in embryonic development from fly to mammals [14]. β-catenin is also crucial for cell cycle progression and for the maintenance of the adherens junctions in epithelia. β-catenin is a proto-oncoprotein, its upregulation being responsible for tumorigenesis in a wide variety of cancers. The fate of the protein is well established as being controlled by phosphorylation of a D-box located at the *N*-termini: phosphorylation at S33, S37, T41 and S45 trigger the poly-ubiquinylation of β-catenin and its subsequent targeting to the 26S proteasome [15]. Therefore, mutations of the D-box or deletions of the N-termini of β-catenin are frequently found in patients' tumors. We have previously demonstrated that *O*-GlcNAcylation of β-catenin reduced its proteasomal susceptibility, particularly modification of T41 with *O*-GlcNAc was found to interfere with the sequential phosphorylation and ubiquitinylation that leads to destruction of this protein [16]. Given these important biological roles and defined functions for specific post-translational modifications, β-catenin appeared to us as the model of choice for the development of our strategy of visualization of specific glycosylated proteins in cells.

2. Results

Among the *in-situ* visualization techniques, the use of GFP and its derivatives is the golden standard to study genetically encoded biomolecules such as proteins. However, for all other non-genetically encoded biomolecules, such as glycans or lipids, GFP-based imaging techniques are not feasible. Therefore, it is necessary to exploit novel techniques to enable visualization of these compounds.

We have opted for a bioorthogonal chemical reporter strategy to detect the *O*-GlcNAc modification state of β-catenin. This technology is based on the incorporation of a chemically modified metabolic precursor of UDP-GlcNAc [16] bearing a pendant bioorthogonal handle at the 2-position of the pyranose ring. This chemically reactive analogue permits conjugation with a fluorophore to generate an imaging probe. This approach allows the *in vivo* study of *O*-GlcNAc modified β-catenin without interfering with native biological processes (Figure 1). The technology we propose involves the dual-labelling of β-catenin with a genetically encoded GFP tag followed by bioorthogonal installation of a second fluorophore on the *O*-GlcNAc unit. The combined use of two fluorescent reporters in close proximity to each other enables a convenient and efficient FRET assay suitable for imaging cells.

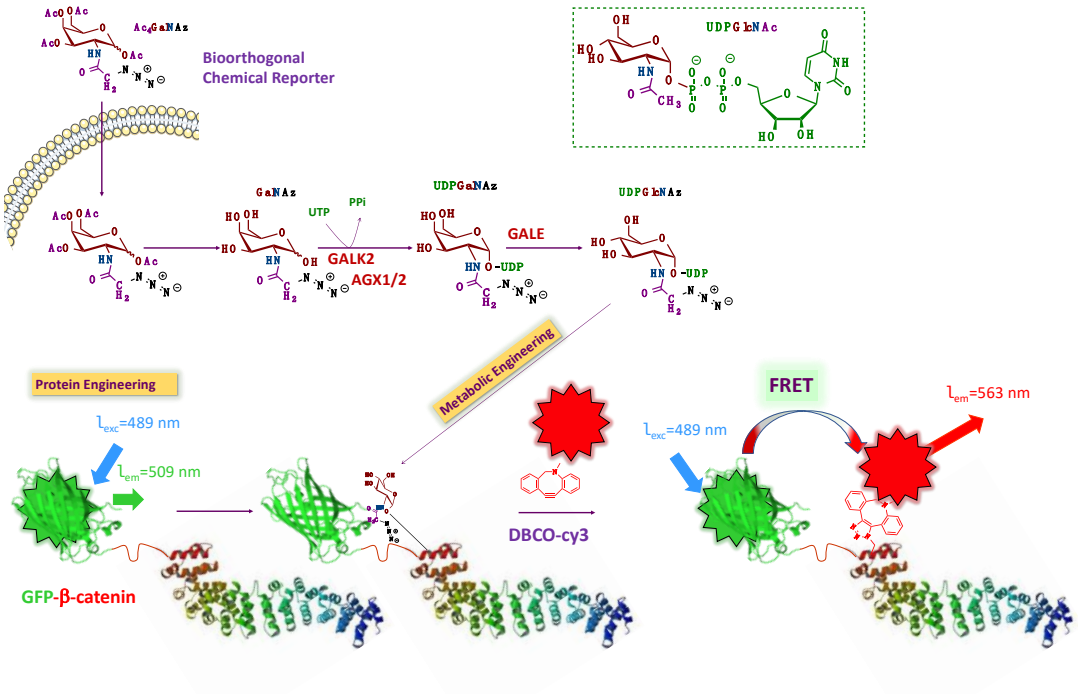

Figure 1. Schematic representation of the strategy: FRET-based imaging of dual labeling of protein and glycans.

β-catenin is genetically labelled with GFP (donor). The intracellular *O*-GlcNAcylated proteins are labelled by metabolic oligosaccharide engineering (MOE) followed by bioorthogonal chemistry with a fluorophore (acceptor). As the distance between donor and acceptor is less than 10 nm, only acceptor bound to the glycans on β-catenin is excited *via* intramolecular FRET.

Briefly, the chemical structure of UDP-GlcNAc is shown in the upper right in Figure 1 (green box). The different colors represent the various metabolic origins of the nucleotide-sugar, as follow: brown, carbohydrate metabolism; blue, glutamine metabolism; purple, metabolism of fatty acids and ketogenic amino acids; green, nucleotide metabolism. The unnatural GlcNAc analog used for our tracing strategy is Ac_4GalNAz (see below). This reporter enters the cell by passive diffusion. Thereafter, Ac_4GalNAz is deacetylated by esterases and then further metabolized to generate UDP-GalNAz. After isomerization into UDP-GlcNAz by the epimerase GALE (UDP-glucose 4-epimerase), OGT transfers GlcNAz to a set of proteins including GFP-β-catenin. The addition of a compatible alkyne-labeled fluorophore results in conjugation of the fluorophore to the azide handle of the GlcNAz unit through a strain-promoted azide-alkyne cycloaddition (SPAAC). This permits FRET between the GFP group and the fluorophore conjugated to the sugar, making it possible to specifically visualize *O*-GlcNAcylated β-catenin in cells.

2.1. Optimization of fusion protein linker

The linker between β-catenin and GFP is an important consideration in order to satisfy the requirements for FRET, including the distance between fluorophore pairs (< 10 nm) and dipole orientation. Therefore, four different fusion proteins were investigated with either no linker or 1-to-3 α-helix linkers (1a, 2a and 3a) inserted between the GFP and the β-catenin domains: (1) GFP-β-catenin, (2) GFP-1a-β-catenin, (3) GFP-2a-β-catenin and (4) GFP-3a-β-catenin (Figure 2a). As a lack of rigidity of these linkers can be a limitation for FRET-based systems [17], a semi-flexible peptide linker $(EAAKEAAAKEAAAKEAAAKA)_{1\text{-}3}$, which adopts an alpha helix conformation, was chosen to bridge the domains. We envisioned this linker would strike a balance in the degee of motility between the two domains, maximizing the potential for efficient FRET.

The different *N*-terminal GFP-tagged β-catenins were produced in HeLa cells and analysed by western blotting in order to assess the expression level of each form (Figure 2b). We found that all four fusion protein constructs were suitably expressed and therefore chose to assess each variant in microscopy experiments. Note that the insertion of linkers increases the apparent molecular weight of GFP-β-catenin depending on the number repeats between the two domains.

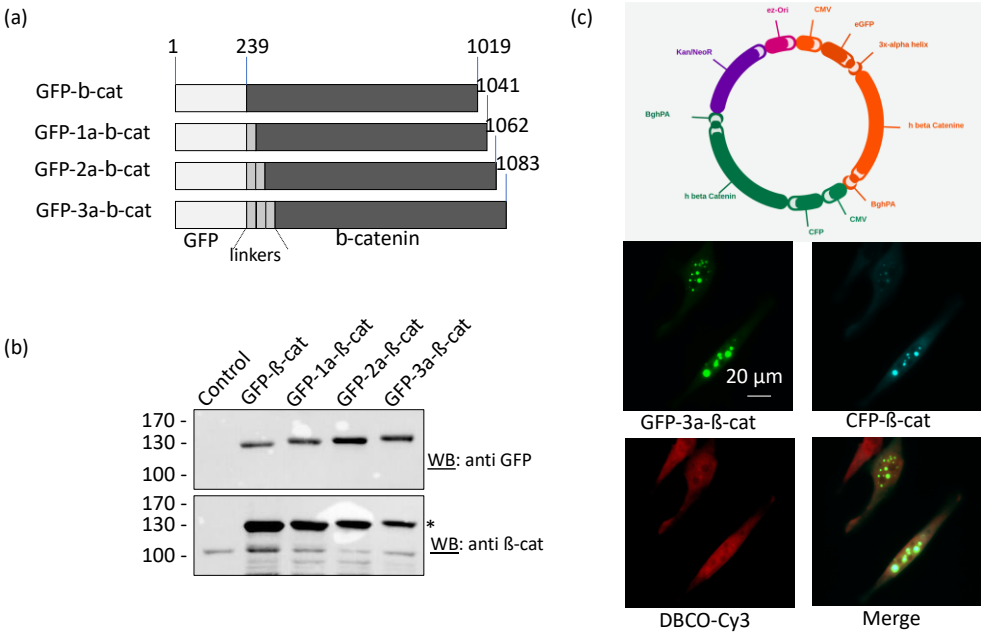

Figure 2 Design and validation of fluorescent β-catenin fusion proteins.
a) Schematic representation of the different GFP-β-catenin constructs used in this study. b) HeLa cells were transfected with the various GFP-β-catenin expressing vectors. Cell lysates were analyzed by western blots using anti-GFP and anti-β-catenin antibodies. The asterisk indicates the detection of the endogenous form of β-catenin. (c) Fluorescence images of HeLa cells expressing GFP-3a–β-catenin and CFP-β-catenin, treated with 200 µM $Ac_4GalNAz$ and labeled with 100 µM DBCO-cy3. The map of the vector encoding both the GFP-3a-β-catenin and the CFP-β-catenin is shown above.

To ensure that FRET will be related to the proximity between donor and acceptor, and not to relative orientation of each modification, we choose the most flexible construct (GFP-3a-β-catenin) for FRET experiments.

Interestingly, a di-systronic expression vector was designed and produced in order to combine the direct synthesis and secretion of both GFP-3a-β-catenin and cyan fluorescent protein β-catenin construct(CFP-β-catenin). Fluorescence colocalization microscopy demosntrated that both proteins localize in the same subcellular compartments (Figures 2c). Therefore, we chose to proceed with the GFP-β-catenin construct in future experiments because to achieve optimal spectral overlap. We also concluded that the length of linker between the GFP and β-catenin domains has no dramatic effect on the integrity of the fusion protein.

2.2. Optimization of metabolic oligosaccharides engineering (MOE)

The ligation reactions used in the metabolic oligosaccharides engineering (MOE) technology are based on the principle of "click chemistry" introduced by the group of Sharpless [18]. A wide range of bioorthogonal reactions has been developed including nucleophilic substitution reactions, carbonyl chemistry and cycloaddition reactions between unsaturated compounds such as Diels-Alder reactions or 1,3-dipolar cycloaddition reactions. Here, we chose the strain-promoted alkyne-azide cycloaddition (SPAAC) due to its ability to label glycans in live cells [19]. Being one of the most widely used cyclooctyne derivative due to its robust stability and reactivity, we selected a fluorophore carrying a dibenzylcyclooctyne (DBCO), also known as ADIBO (azadibenzocyclooctyne) or DIBAC (dibenzoazacyclooctyne) [20].

As *N*-azidoacetylglucosamine (GlcNAz) turned out to be a weak metabolic labeling reagent [16], we instead used *N*-azidoacetylgalactosamine (GalNAz) which is more efficiently metabolized into UDP-N-GlcNAz in cells. In its peracetylated form (Ac_4GalNAz), this derivative has the property of being cell-permeable.

To address the optimum Ac_4GalNAz concentration for cell labeling and FRET analysis, HeLa cells were treated with increasing Ac_4GalNAz concentration (10, 20, 50, 100 and 200 μM) to introduce the *O*-GlcNAz onto intracellular *O*-GlcNAcylated proteins. The azidosugar was then labeled with the with DBCO-cy3 FRET acceptor (100 μM) using the SPAAC reaction, permitting visualization of *O*-GlcNAz modified β-catenin. Colocalization of green and red signals produced a yellow color, validating the dual labeling (figure 3).

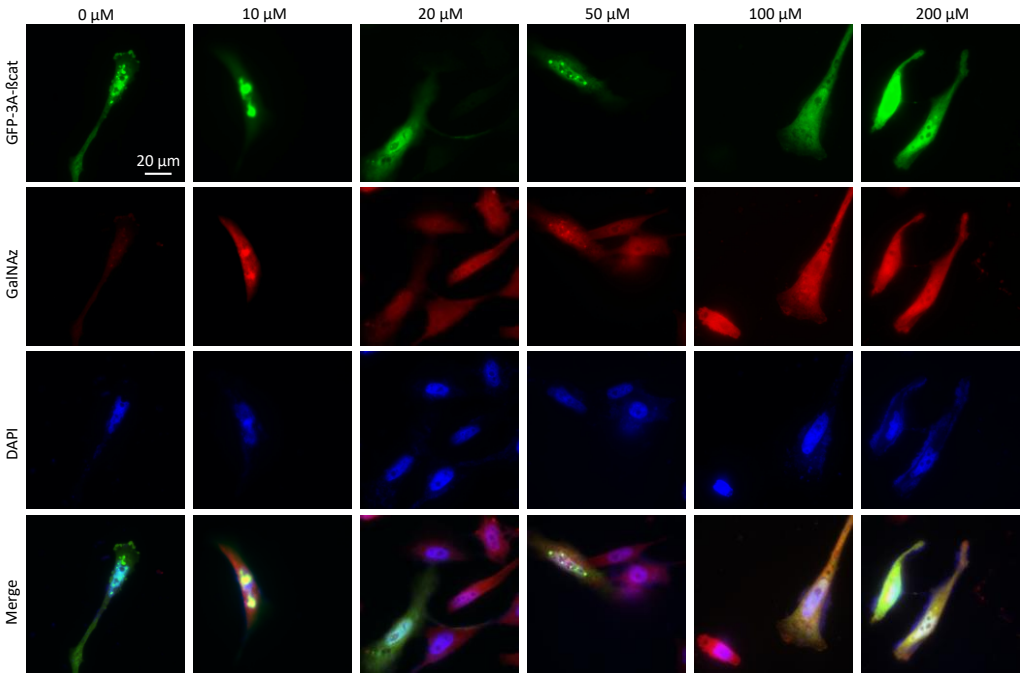

Figure 3. Optimization of the concentration of the chemical reporter.
HeLa transfected with the GFP-3a-β-catenin expressing vectors were treated with increasing Ac_4GalNAz concentration (10, 20, 50, 100 and 200 μM) and labeled with DBCO-cy3 (10 μM).

As shown in Figure 3, no modification of the morphology of the cells was observed even at the highest dose of 200 μM of the chemical reporter showing that the the toxicity of the azidosugar concentration is very negligible even at the highest concentrations. Acetic acid release inside cells upon enzymatic deacetylation of Ac_4GalNAz did not seem to induce cytotoxicity as was previously reported for Ac_4ManNAz (>50 μM) [21]. In order to promote high FRET efficiencies, we chose the highest Ac_4GlcNAz concentration of 200 μM.

2.3. SLiM-FRET readout assay

To carry out a quantitative analysis of the FRET between the GFP and the cy3-labeled GlcNAc, a Spectral fluorescence Lifetime imaging Microscopy (SLiM) acquisition system was used, permitting unambiguous FRET measurements (Figure 4a). In the absence of the chemical reporter, a mean τ value (τ_m) of 2.8+/- 0.06 ns was observed in GFP-3a-β-catenin-expressing cells (Figure 4b).
We then imaged GFP-3a-β-catenin expressing cells that were treated with Ac_4GalNAz and click-labeled with DBCO-cy3. Using these conditions, the τ_m value of the GFP reporter in Ac_4GalNAz-treated cells decreased to 2.5+/-0.17 ns (Figure 4b). A FRET event can thus be observed with a p value <0.05.

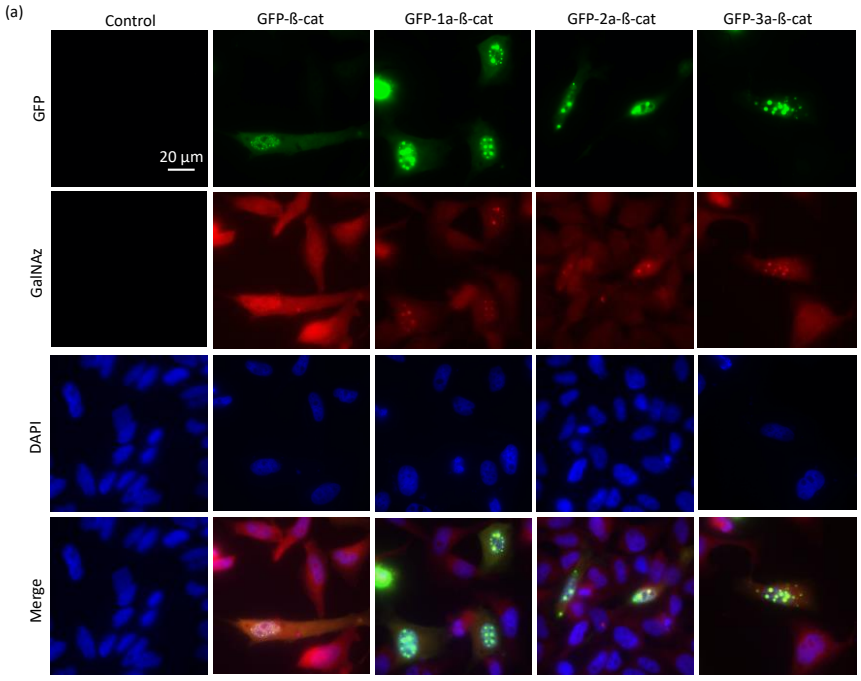

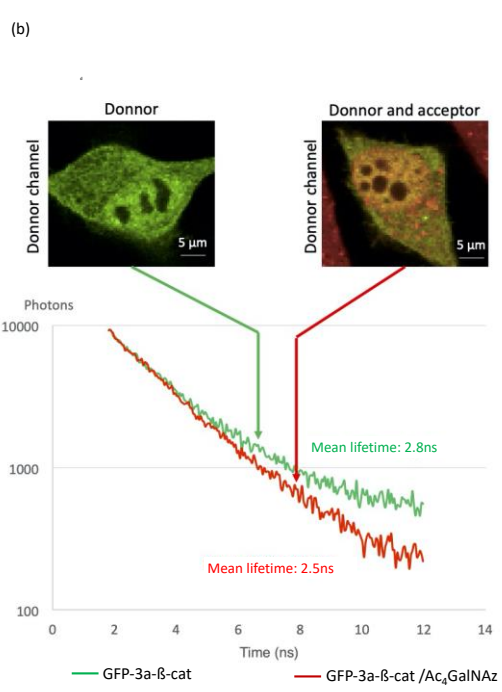

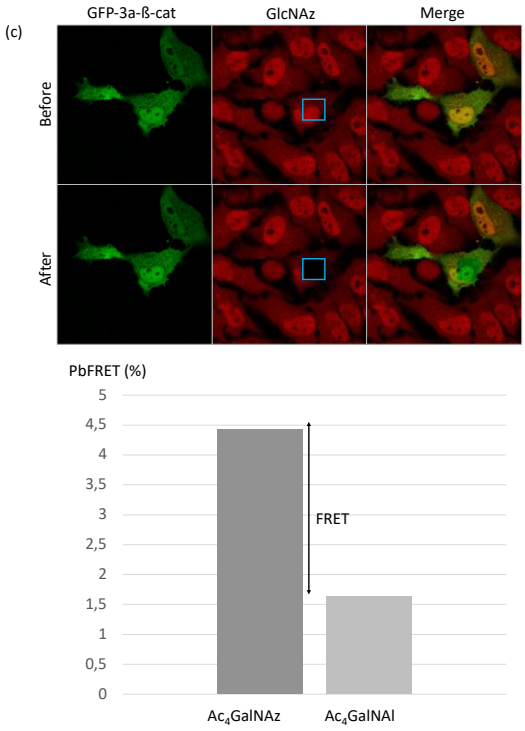

Figure 4. Proof of feasibility: FRET imaging of *O*-GlcNAcylated GFP-3a-β-catenin
(a) Fluorescence images of HeLa cells expressing GFP-linker-β-catenins, treated with 200 µM Ac_4GalNAz and labeled with DBCO-cy3. (b) SLiM-FRET experiment using two-photon excitation: representative photon decay curves and associated fluorescence mean lifetime extracted from only the GFP emission channel. (c) Donor dequenching after acceptor photobleaching. The inserted blue box indicates the photobleached area. Histograms correspond to calculated pb-FRET inside the cells after photobleaching.

These experiments allowed us to observe variations up to 300 picoseconds in lifetime experiments. This range corresponds to a deviation from GFP-3a-β-catenin basal *O*-GlcNAcylation level to the non-*O*-GlcNAcylated state. This dynamic range is sufficient to decipher subtle variations in *O*-GlcNAcylation levels.

We have thus demonstrated that our device associating GFP-3a-β-catenin GalNAz-cy3 SLiM-FRET strategy is sufficiently sensitive for use in live cells. This important point at this level of the study can be considered as a proof of concept for this new tool.

2.4. Pb-FRET readout assay

While SLiM allows quantitative and sensitive FRET measurements, it requires a dedicated acquisition system and is highly time-consuming. After validation of the biosensor using SLiM, we wanted to demonstrate the robustness of our method using a traditionnal confocal microscope to monitore FRET through a photobleaching FRET readout assay, a fast and widely available technology.

As depicted in Figure 4c, DBCO-cy3 was specifically photobleached within a defined region of the cell in order to keep an internal control [23]. Using pb-FRET, we observed a measurable FRET efficiency of 4.4+/-0.1 on GFP-3a-β-catenin expressing cells when treated with Ac_4GalNAz and click-labeled with DBCO-cy3.

In order to confirm that measured FRET resulted from intramolecular FRET, we performed control experiments with GFP-3a-β-catenin and the alkyne-containing reporter Ac_4GalNAl [23]. This analogue is unable to react with DBCO-cy3, allowing evaluation of the possible contributions from intermolecular FRET between the two fluorophores. More than a thousand intracellular proteins are post-translationally modified with *O*-GlcNAc and thus susceptible to incorporation of GlcNAz followed by DBCO-cy3. However, maintaining low expression of GFP-β-catenin and concentration of cy3 in a 3D environment induces a statistically neglectable amount of donor and acceptors in close vicinity [24]. No measurable FRET compared to GFP-β-catenin alone was monitored as confirmed by experiments presented in Figure 4c. Indeed, a low background signal of 1.2 +/-0.5 was recorded when cells were treated with Ac_4GalNal.

2.5. Pharmacology

Having developped an efficient, robust and easy to use technique to process Hela cells for pb-FRET imaging, we used this approach to evaluate the pharmacological effects of thiamet-G and $Ac_4$5SGlcNAc. Thiamet-G [25] and $Ac_4$5SGlcNAc [16] are effective cell active inhibitors of *O*-GlcNAcase (OGA) and *O*-GlcNAc transferase (OGT) respectively. OGT catalyzes the addition of *O*-GlcNAc to proteins [26], OGA removes the modification [27]. Thiamet-G is a potent (in vitro K_i = 2.1 nM, cell-based EC_{50} = 21 nM) stable mimic of the oxazoline-like transition state used by OGA active site during the OGA-catalyzed hydrolysis of *O*-GlcNAc leading to an increase of *O*-GlcNAc modification of proteins. Within cells, the prodrug $Ac_4$5SGlcNAc generates the OGT inhibitor UDP-5SGlcNAc (in vitro K_i = 5 μM) within cells and decreases cellular *O*-GlcNAcylation , (cell-based EC_{50} = 5 μM). Both compounds have been evaluated in SK-N-AS cells for imaging the changes of tau *O*-GlcNAc [12], to the best of our knowledge this is the first study to compare the inhibitory effect of thiamet-G and $Ac_4$5SGlcNAc upon *O*-GlcNAcylation on β-catenin in living cells.

When GFP-3a-β-catenin-transfected HeLa cells were treated with 1 µM thiamet-G 2 hours before or after incubation with 200 µM Ac_4GalNAz, and finally labeled with DBCO-cy3 a decrease of the pb-

FRET signal was recorded consitent with a higher rate of occupancy of *O*-GlcNAc moieties on β-catenin in response to OGA inhibition.

Conversely, when GFP-3a-β-catenin-transfected HeLa cells were incubated with 100 μM $Ac_4$5SGlcNAc for 2 h prior to the treatment with Ac_4GalNAz and labeled with DBCO-cy3, a large increase (2.1 %; see Figure 5) of the pb-FRET signal was recorded compared to untreated cells. This observation is consistent with previous studies [26-28], that showed a major reduction in cellular O-GlcNAc when using this inhibitor. Indeed, the expression of OGT increases in response to its inhibition. Thus the blockade of its activity by UDP-5SGlcNAc results, as expected, in higher OGT expression as previously demonstratedand also seen with the OGT inhibitor OSMI-1 [28], or upon glucose deprivation [29,30]. It should also be noted here that the substrate is present in an excess amount compared to the inhibitor in our step-up, as Ac_4GalNAz concentration is higher than $Ac_4$5SGlcNAc concentration, and effective inhibition nevertheless still occurs. On the other hand adding the OGT inhibitor after treating the cells with Ac_4GalNAz had no effect, the same pb-FRET signal being recorded as that of the control cells incubated only with the azido-sugar. The absence of increase in signal is most likely due to the fact that the incubation time with the inhibitor is too short to observe an increase in expression of OGT as we assume for the previous condition.

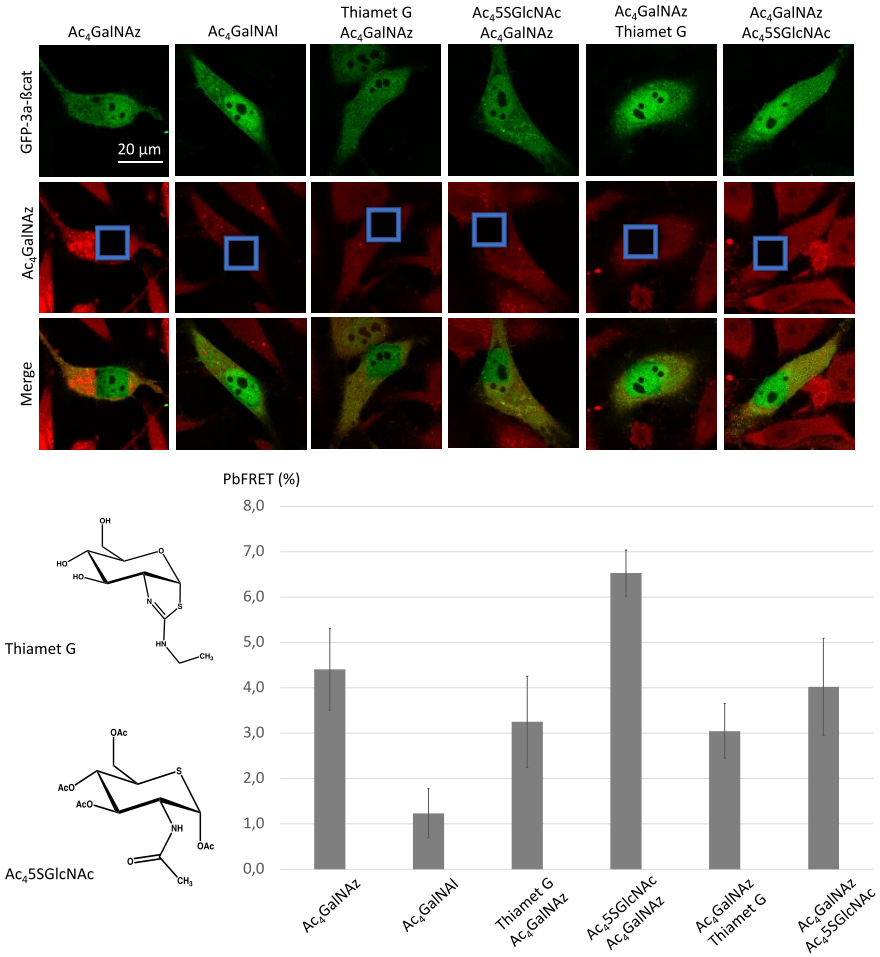

Figure 5. Imaging the changes of pb-FRET for GFP-3a-β-catenin in HeLa cells induced by the OGT and OGA inhibitors.

(a) Fluorescence images of the *O*-GlcNAcylated glycoform of β-catenin before and after photo-bleaching using thiamet-G or $Ac_4$5SGlcNAc. (b) Histograms corresponding to calculated pb-FRET inside the cells after photobleaching using thiamet-G or $Ac_4$5SGlcNAc.

3. Discussion

The Human Genome project consortium revealed that human DNA coded for only a third of the 100,000 genes expected [31]. Since then, this number is continuing to be lowered with a current estimate of about 21,000 genes. Yet, the human proteome is very broad since it is estimated capable of regulating more than 500 million different biological activities [32]. In addition to the mechanisms of alternative splicing of the transcribed primary proteins, post-translational modifications increase exponentially the number of possible protein isoforms [4]. These PTMs alter proteins functions through various mechanisms such as changes in protein-protein interactions, altered stability or adaptation of catalytic activity to the environmental context. Owing to the vast diversity and the complexity of PTMs, studying them is usually challenging; the difficulty comes with the specific tagging of one precise form of the protein of interest and to the lack of imaging tools to permit tracking of this protein form [3,6,10,12]. In this regard, the FRET technologies described in this work may help with visualizing the glycosylation state of specific glycoproteins and also provide the bases for characterizing glycomes with molecular precision.

Our present work refers to the specific *O*-GlcNAcylation PTM that occurs mostly intracellularly. Indeed, *O*-GlcNAcylation regulates a large set of biological functions in a nutrient-dependent manner [34]. Dysregulation of *O*-GlcNAcylation processes are observed in a variety of diseases including neurodegenerative diseases, metabolic disorders, cardiovascular disorders and cancers.
A better understanding of *O*-GlcNAcylation function, protein by protein, would certainly translate in significant progress in knowledge and treatment of these diseases. However, there are few existing molecular tools that allows a rapid and easy determination of the *O*-GlcNAcylation status of a protein of interest in live cells, rendering such progresses difficult to make.

In this study, we successfully adapted the dual labeling method initially developed by Lin and co-workers [12] to detect a β-catenin glycoform using FRET techniques. As the selection of a suitable linker of GFP-tagged proteins is often neglected and underexplored, we focused a part of our study in the design and the choice of the linker between GFP and β-catenin. As FRET is contingent upon the ability to precisely introduce a suitable pair of donor and acceptor fluorophores into the protein of interest, we concomitantly optimized not only the linker but also the chemical reporter concentration. We validated our approach using a combination of azido sugar labeling and two-photon fluorescence life time imaging spectroscopy (SLiM). As a negative control, we also used an alkyne sugar analogue (which is unable to react with the selected fluorophore via a SPAAC reaction) to confirm intramolecular FRET. Thereafter, we turned our attention to demonstrate the robustness of our technology using a conventional confocal microscope to monitor FRET through a pb-FRET readout assay. With this technology in our hands, we evaluated changes of β-catenin O-GlcNAcylation by inhibiting OGA or OGT. Finally, we provided a flowchart demonstrating how these technologies could be meaningfully combined (Figure 6).

This methodology, developed on a precise cell system, protein and PTM, should open up interesting perspectives in various fields of cell biology. This system should be fairly easily adaptable to any type of glycosylation given that MOE is an established technology with a broad scope of sugars that can be incorporated *in vitro*. We also expect that in the future, this strategy will be useful for the study of other PTMs after the requisite optimization towards a particular type of modification. In view of the speed of coordination between chemists and biologists, such tools should soon emerge for many modifications other than glycosylations.

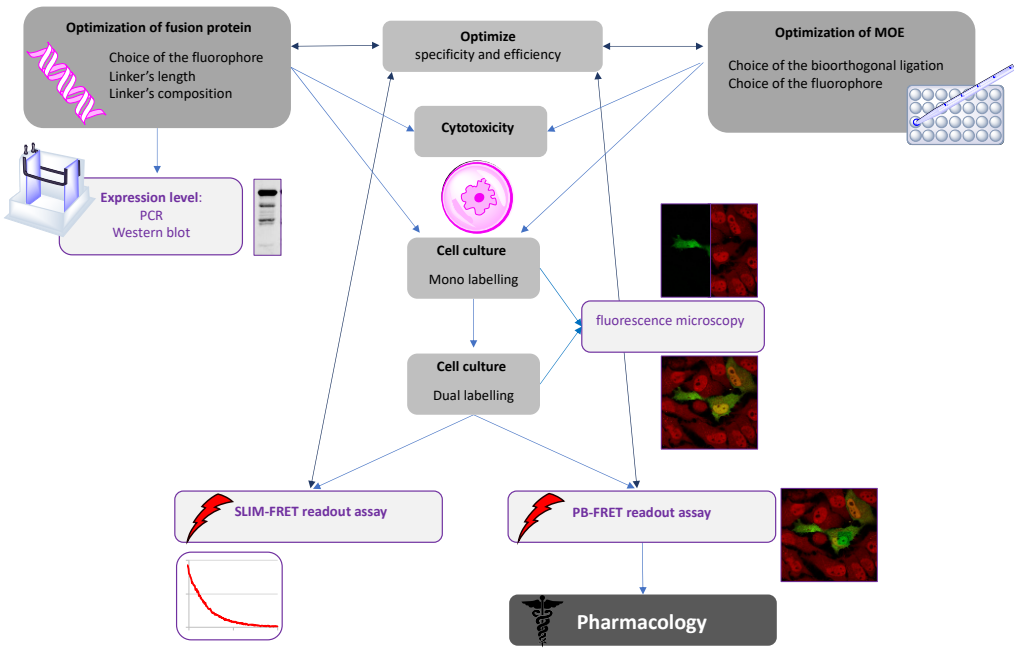

Figure 6. Flowchart demonstrating how to combine the technologies for FRET-based imaging of dual labeling of glycoproteins

4. Materials and Methods

4.1. Chemical compounds

Ac_4GalNAz, Ac_4GAlNAl and DBCO-Cy3 were purchased from Click Chemistry Tools (Scottsdale, USA). Thiamet-G and $Ac_4$5SGlcNAc were prepared as previously described [25,33].

4.2. Cell culture

HeLa cells were obtained from the American Tissue Culture Collection. Cells were grown in Dulbecco's modified Eagle's medium (Lonza) supplemented with 10% (v/v) of fetal calf serum (Lonza). Cells were maintained at 37°C in a humidified atmosphere containing 5% (v/v) CO_2.

4.3. Plasmids

vCMVp-GFP-ß-catenin, vCMVp-GFP-1a-ß-catenin, vCMVp-GFP-2a-ß-catenin, vCMVp-GFP-3a-ß-catenin, vCMVp-GFP-3A-ß-catenin-CFP-ß-catenin were generated by e-Zyvec (www.e-zyvec.com, Loos, France). Linkers between GFP and ß-catenin are an alanine-rich amino acid sequence repeated one, two or three times: 5'- EAAAKEAAAKEAAAKEAAAKA -3'.

4.4. Transfections

For microscopy, cells were grown on glass coverslips and transfected at 70% confluency. Transfections were performed using 1µL of Jetoptimus (Polyplus), 1µg of plasmid in 900µL DMEM according to manufacturer's instruction. Transfections mix was replaced 4 hours later with fresh medium containing Ac_4GAlNAz or Ac_4GalNAl (200 µM), with or without $Ac_4$5SGlcNAc (100 µM) or Thiamet G (1 µM), for 24 hours.

4.5. Western blot analyses

Cells were washed once in ice-cold PBS and lysed in RIPA buffer (Tris/HCL 50mM, NaCl 150 mM, NP40 0,5% (v/v), EDTA 1 mM, Na_3VO_4 1mM, NaF 5 mM, pH 7.9) supplemented with a protease inhibitors mix (Roche Diagnostics) for 20 minutes on ice. Lysate were centrifuged at 5000 RPM, 4°C for 10 min and supernatants were collected. Protein quantitation was determined by using the BCA assay (ThermoFischer). Equal quantities (15-20 µg) of proteins were loaded and separated by 10% SDS-PAGE. Proteins were transferred onto nitrocellulose membrane (GE Healthcare) at 200 mA for 2 hours.

Membranes were blocked for 1 h at room temperature with 5% (w/v) nonfat dry milk in Tris-buffered saline (TBS) Tween (TBST) buffer (15 mM Tris, 140 mM NaCl, 0.05% (v/v) Tween20, pH 8.0). Membranes were incubated overnight at 4°C with anti ß-catenin (1:2000) (H102, Santa Cruz Biotechnology, Santa Cruz, CA, USA) or anti GFP (1:1000) monoclonal antibodies. After three washes with TBST, membranes were incubated with corresponding secondary HRP-linked antibodies (1:10,000 in TBST) for 1h at room temperature. After three washes in TBST, detection was performed with a CCD camera (Fusion Solo, Vilber Lourmat).

4.6. Sample preparation and bioothogonal ligation for fluorescence microscopy

Cells cultured on coverslips were washed three times in Dulbecco's Phosphate Buffer Saline (Lonza) containing calcium and magnesium. Cells were fixed with 4% (w/v) paraformaldehyde (pH 7.3) for 30 min at room temperature and washed with ice-cold PBS thrice. Coverslips were switched in a humid chamber. For SPAAC, 10µM DBCO-Cy3 was applied for 1 hour. Cells were washed three times with ice-cold PBS and coverslips were mounted in mounting medium (Dako).

4.7. Spectral fluorescence lifetime imaging microscopy

Lifetime measurements were performed using a MW-FLIM detector and a SPC 150 photocounting card from Becker & Hickl (Becker & Hickl, Berlin, Germany) adapted on a laser scanning microscope LSM 710 NLO Zeiss (Zeiss SAS, Germany) and coupled with a Chameleon TiSa accordable 80 MHz pulsed laser (COHERENT, USA). For more details on acquisition and analysis procedure for FRET, please see [34]. For GFP lifetime measurements, acquisitions were performed at 860 nm and detection between 500 and 560 nm. Lifetime values were extracted from a minimum of 10 cells per experiment.

4.8. Photobleaching FRET

The samples were observed under A1 Nikon confocal microscope with a 60X Oil immersion objective. The green fluorescence (GFP) was acquired with λex = 488 nm and λ_{em} = 500-530 nm and the red fluorescence (Cy3) was acquired with λex= 561.6 nm and λ_{em}=570-620 nm. Photobleaching of the acceptor was achieved by increasing laser power from 10% to 100%, increasing the zoom from 1 to 16 and by scanning the selected area 10 time. Images acquired before and after photobleaching were processed according to [22] with ImageJ. Photobleaching FRET values were extracted from a minimum of 10 cells per experiment.

Author Contributions: Conceptualization, C.B. and T.L.; methodology, A.K., C.S., C.T., M.A., T.L. and C.B.; writing—original draft preparation, A.K., C.S., T.L. and C.B.; writing—review and editing, A.K., C.S., T.L. and C.B.; funding acquisition, T.L. and C.B. All authors have read and agreed to the published version of the manuscript.

Funding: This study was supported by the French government through the Programme Investissement d'Avenir (I-SITE ULNE / ANR-16-IDEX-0004 ULNE) managed by the Agence Nationale de la Recherche.

Acknowledgments: The different four expression vectors were synthesized by e-Zyvec. (www.e-zyvec.com). We are indebted to "UMS 2014 - US 41 - Plateformes Lilloises en Biologie & Santé" for providing the technical environment conducive to achieving this work. Pr. David Vocadlo is acknowledged for helpful discussion.

Conflicts of Interest: The authors declare no conflict of interest.

References

1. Varki, A., Cummings, R.D., Esko, J.D., Stanley, P., Hart, G.W., Aebi, M., Darvill, A.G., Kinoshita, T., Packer, N.H., Prestegard, J.H., Schnaar, R.L., Seeberger, P.H., Eds.; Essentials of Glycobiology; 3rd ed.; Cold Spring Harbor Laboratory Press: Cold Spring Harbor (NY), 2015.

2. Silsirivanit, A. Glycosylation markers in cancer. *Adv Clin Chem* **2019**, *89*, 189–213, doi:10.1016/bs.acc.2018.12.005.

3. Haga, Y.; Ishii, K.; Hibino, K.; Sako, Y.; Ito, Y.; Taniguchi, N.; Suzuki, T. Visualizing specific protein glycoforms by transmembrane fluorescence resonance energy transfer. *Nat Commun* **2012**, *3*, 1–7, doi:10.1038/ncomms1906.

4. Yang, X.; Qian, K. Protein O-GlcNAcylation: emerging mechanisms and functions. *Nat. Rev. Mol. Cell Biol.* **2017**, *18*, 452–465, doi:10.1038/nrm.2017.22.

5. King, D.T.; Males, A.; Davies, G.J.; Vocadlo, D.J. Molecular mechanisms regulating O-linked N-acetylglucosamine (O-GlcNAc)-processing enzymes. *Curr Opin Chem Biol* **2019**, *53*, 131–144, doi:10.1016/j.cbpa.2019.09.001.

6. Dube, D.H.; Bertozzi, C.R. Metabolic oligosaccharide engineering as a tool for glycobiology. *Curr Opin Chem Biol* **2003**, *7*, 616–625, doi:10.1016/j.cbpa.2003.08.006.

7. Gross, H.J.; Brossmer, R. Enzymatic introduction of a fluorescent sialic acid into oligosaccharide chains of glycoproteins. *Eur. J. Biochem.* **1988**, *177*, 583–589, doi:10.1111/j.1432-1033.1988.tb14410.x.

8. Wratil, P.R.; Horstkorte, R.; Reutter, W. Metabolic Glycoengineering with N-Acyl Side Chain Modified Mannosamines. *Angew. Chem. Int. Ed. Engl.* **2016**, *55*, 9482–9512, doi:10.1002/anie.201601123.

9. Gilormini, P.A.; Lion, C.; Vicogne, D.; Guérardel, Y.; Foulquier, F.; Biot, C. Chemical glycomics enrichment: imaging the recycling of sialic acid in living cells. *Journal of Inherited Metabolic Disease* **2018**, *41*, 515–523, doi:10.1007/s10545-017-0118-3.

10. Belardi, B.; de la Zerda, A.; Spiciarich, D.R.; Maund, S.L.; Peehl, D.M.; Bertozzi, C.R. Imaging the Glycosylation State of Cell Surface Glycoproteins by Two-Photon Fluorescence Lifetime Imaging Microscopy. *Angew. Chem. Int. Ed. Engl.* **2013**, *52*, 14045–14049, doi:10.1002/anie.201307512.

11. Lin, W.; Du, Y.; Zhu, Y.; Chen, X. A cis-membrane FRET-based method for protein-specific imaging of cell-surface glycans. *J. Am. Chem. Soc.* **2014**, *136*, 679–687, doi:10.1021/ja410086d.

12. Lin, W.; Gao, L.; Chen, X. Protein-Specific Imaging of O-GlcNAcylation in Single Cells. *ChemBioChem* **2015**, *16*, 2571–2575, doi:10.1002/cbic.201500544.

13. Doll, F.; Buntz, A.; Späte, A.-K.; Schart, V.F.; Timper, A.; Schrimpf, W.; Hauck, C.R.; Zumbusch, A.; Wittmann, V. Visualization of Protein-Specific Glycosylation inside Living Cells. *Angew. Chem. Int. Ed. Engl.* **2016**, *55*, 2262–2266, doi:10.1002/anie.201503183.

14. Clevers, H.; Nusse, R. Wnt/β-catenin signaling and disease. *Cell* **2012**, *149*, 1192–1205, doi:10.1016/j.cell.2012.05.012.

15. Liu, C.; Li, Y.; Semenov, M.; Han, C.; Baeg, G.-H.; Tan, Y.; Zhang, Z.; Lin, X.; He, X. Control of β-Catenin Phosphorylation/Degradation by a Dual-Kinase Mechanism. *Cell* **2002**, *108*, 837–847, doi:10.1016/S0092-8674(02)00685-2.

16. Boyce, M.; Carrico, I.S.; Ganguli, A.S.; Yu, S.-H.; Hangauer, M.J.; Hubbard, S.C.; Kohler, J.J.; Bertozzi, C.R. Metabolic cross-talk allows labeling of O-linked β-N-acetylglucosamine-modified proteins via the N-acetylgalactosamine salvage pathway. *PNAS* **2011**, *108*, 3141–3146, doi:10.1073/pnas.1010045108.

17. Chen, X.; Zaro, J.L.; Shen, W.-C. Fusion protein linkers: property, design and functionality. *Adv. Drug Deliv. Rev.* **2013**, *65*, 1357–1369, doi:10.1016/j.addr.2012.09.039.

18. Kolb, H.C.; Finn, M.G.; Sharpless, K.B. Click Chemistry: Diverse Chemical Function from a Few Good Reactions. *Angew. Chem. Int. Ed. Engl.* **2001**, *40*, 2004–2021, doi:10.1002/1521-3773(20010601)40:11<2004::aid-anie2004>3.3.co;2-x.

19. Jewett, J.C.; Bertozzi, C.R. Cu-free click cycloaddition reactions in chemical biology. *Chem. Soc. Rev.* **2010**, *39*, 1272–1279, doi:10.1039/B901970G.

20. Kuzmin, A.; Poloukhtine, A.; Wolfert, M.A.; Popik, V.V. Surface Functionalization Using Catalyst-Free Azide−Alkyne Cycloaddition. *Bioconjugate Chem.* **2010**, *21*, 2076–2085, doi:10.1021/bc100306u.

21. Sang-Soo, H.; Dong-Eun, L.; Hye-Eun, S.; Sangmin, L.; T, J.; Jung-Hwa, O.; Hyang-Ae, L.; Sung-Hwan, M.; Jongho, J.; Seokjoo, Y.; et al. Physiological Effects of Ac4ManNAz and Optimization of Metabolic Labeling for Cell Tracking. *Theranostics* **2017**, *7*, 1164–1176, doi:10.7150/thno.17711.

22. Camuzeaux, B.; Spriet, C.; Héliot, L.; Coll, J.; Duterque-Coquillaud, M. Imaging Erg and Jun transcription factor interaction in living cells using fluorescence resonance energy transfer analyses. *Biochem Biophys Res Commun* **2005**, *332*, 1107–1114, doi:10.1016/j.bbrc.2005.05.057.

23. Batt, A.R.; Zaro, B.W.; Navarro, M.X.; Pratt, M.R. Metabolic Chemical Reporters of Glycans Exhibit Cell-Type-Selective Metabolism and Glycoprotein Labeling. *Chembiochem* **2017**, *18*, 1177–1182, doi:10.1002/cbic.201700020.

24. Sipieter, F.; Vandame, P.; Spriet, C.; Leray, A.; Vincent, P.; Trinel, D.; Bodart, J.-F.; Riquet, F.B.; Héliot, L. From FRET imaging to practical methodology for kinase activity sensing in living cells. *Prog Mol Biol Transl Sci* **2013**, *113*, 145–216, doi:10.1016/B978-0-12-386932-6.00005-3.

25. Yuzwa, S.A.; Macauley, M.S.; Heinonen, J.E.; Shan, X.; Dennis, R.J.; He, Y.; Whitworth, G.E.; Stubbs, K.A.; McEachern, E.J.; Davies, G.J.; et al. A potent mechanism-inspired O-GlcNAcase inhibitor that blocks phosphorylation of tau in vivo. *Nat. Chem. Biol.* **2008**, *4*, 483–490, doi:10.1038/nchembio.96.

26. Haltiwanger, R.S.; Holt, G.D.; Hart, G.W. Enzymatic addition of O-GlcNAc to nuclear and cytoplasmic proteins. Identification of a uridine diphospho-N-acetylglucosamine:peptide beta-N-acetylglucosaminyltransferase. *J. Biol. Chem.* **1990**, *265*, 2563–2568.

27. Dong, D.L.; Hart, G.W. Purification and characterization of an O-GlcNAc selective N-acetyl-beta-D-glucosaminidase from rat spleen cytosol. *J. Biol. Chem.* **1994**, *269*, 19321–19330.

28. Decourcelle, A.; Loison, I.; Baldini, S.; Leprince, D.; Dehennaut, V. Evidence of a compensatory regulation of colonic O-GlcNAc transferase and O-GlcNAcase expression in response to disruption of O-GlcNAc homeostasis. *Biochem Biophys Res Commun* **2020**, *521*, 125–130, doi:10.1016/j.bbrc.2019.10.090.

29. Cheung, W.D.; Hart, G.W. AMP-activated Protein Kinase and p38 MAPK Activate O-GlcNAcylation of Neuronal Proteins during Glucose Deprivation. *J Biol Chem* **2008**, *283*, 13009–13020, doi:10.1074/jbc.M801222200.

30. Taylor, R.P.; Geisler, T.S.; Chambers, J.H.; McClain, D.A. Up-regulation of O-GlcNAc Transferase with Glucose Deprivation in HepG2 Cells Is Mediated by Decreased Hexosamine Pathway Flux. *J Biol Chem* **2009**, *284*, 3425–3432, doi:10.1074/jbc.M803198200.

31. Venter, J.C.; Adams, M.D.; Myers, E.W.; Li, P.W.; Mural, R.J.; Sutton, G.G.; Smith, H.O.; Yandell, M.; Evans, C.A.; Holt, R.A.; et al. The sequence of the human genome. *Science* **2001**, *291*, 1304–1351, doi:10.1126/science.1058040.

32. Ho, B.; Baryshnikova, A.; Brown, G.W. Unification of Protein Abundance Datasets Yields a Quantitative Saccharomyces cerevisiae Proteome. *Cell Systems* **2018**, *6*, 192-205.e3, doi:10.1016/j.cels.2017.12.004.

33. Gloster, T.M.; Zandberg, W.F.; Heinonen, J.E.; Shen, D.L.; Deng, L.; Vocadlo, D.J. Hijacking a

biosynthetic pathway yields a glycosyltransferase inhibitor within cells. *Nat. Chem. Biol.* **2011**, *7*, 174–181, doi:10.1038/nchembio.520.

34. Terryn, C.; Paës, G.; Spriet, C. FRET-SLiM on native autofluorescence: a fast and reliable method to study interactions between fluorescent probes and lignin in plant cell wall. *Plant Methods* **2018**, *14*, 74, doi:10.1186/s13007-018-0342-3.